Citation: Lee, K., Kriesel, J, and Gat, N., "Night Vision Camera Fusion with Natural Colors Using a Spectral / Texture Based Material Identification Algorithm," Meeting of the Military Sensing Symposia (MSS) on Passive Sensors, February 23, 2010, Orlando, FL

Night Vision Camera Fusion with Natural Colors Using a Spectral / Texture Based Material Identification Algorithm

February 2010
K. Lee, J. Kriesel, and N. Gat
Opto-Knowledge Systems, Inc. (OKSI)
19805 Hamilton Ave. Torrance CA 90502

ABSTRACT

Combining multiple types of night vision cameras, such as low-light-level visible to near infrared (VNIR), short-wave (SWIR), mid-wave (MWIR), and/or long-wave infrared (LWIR), enables the presentation of complimentary information into a single display. A great deal of developmental work has been devoted to maximizing the information in the fused imagery; however, fusion schemes that rely on some form of mapping or transformation from the multi-band imagery to a composite false-color image do not consistently match recognizable "true" colors and also suffer from color consistency problems as the environment and materials in the scene change. Other related techniques that have proven useful for mapping single band grayscale values to a pseudo-color palette have limited utility for multi-band infrared systems, particularly in dynamic environments where the distribution of brightness values can change.

This paper presents a method for combining night vision imagery from multiple cameras into a single fused output with recognizable colors. The colors are determined through a material identification algorithm that relies on a spectral/texture analysis along with additional ancillary information. The calculations are done in a probabilistic manner using a knowledge-based inference technique that considers material database matching together with expected scene content, available via future Global Information Grids and Geographical Information Grid Services. The result is that identified materials can be rendered in natural recognizable colors (e.g., grass is green), which aides in scene understanding, object identification, and also reduces viewer fatigue.

Introduction

Night vision technology has evolved over the past few decades in two directions: (i) reflective light sensitive devices (e.g., I2 tubes, InGaAs, and EMCCD), and (ii) thermal infrared detection systems that are sensitive to heat. Reflective devices provide a more perceptually comprehensive image of the scene while thermal ones enable detection of persons, machinery, animals, etc., in the absence of reflected light. However, since both systems typically produce monochrome imagery, neither of the systems capture the additional information that can be utilized by human color vision for scene understanding. Many studies have shown that scene understanding, reaction time and object identification are faster and more accurate with color imagery than with monochrome imagery [1], [2].

A great deal of work has been devoted to develop various methods for colorizing monochrome night vision imagery captured either in a single band or multiple bands. Hogervorst and Toet presented an algorithm [3] using daytime reference image mapping to colorize a single band nighttime target image. Though the algorithm mimics true color rendering, it works only on limited scenes, which include similar content to a reference image. To overcome the limitation of the single band approach, multi-band approaches have been developed that utilize imagery from multiple types of cameras such as visible to near IR (VNIR), short-wave IR (SWIR), mid-wave IR (MWIR), and/or long-wave (thermal) IR (LWIR/TIR). Toet and Walraven [4] introduced a mapping method to generate false color image through multi-band fusion. Though this method renders the fused imagery in a color form to maximize the scene information, it does not match recognizable true color, which causes color consistency to be difficult to maintain as the environment and materials in the scene change. Fay *et-al* [5] developed an algorithm using multi-sensor imagery based on biological neural network mapping models of the spatial and opponent-color processes in human retina and visual cortex. This technique attempted true color, but still suffers from producing false color imagery that can vary with different environmental conditions.

Due to the lack of color information (e.g., RGB chroma) during the nighttime, none of these mapping based techniques described above produce a consistent true color rendering. Hence, the problem of creating true color imagery should be dealt with by some other form of image analysis. In general, the background objects in the scene tend to show their unique colors independent of environmental changes. If the background objects can be recognized in the scene image, the objects can be mapped and colorized using their natural colors (e.g., tree is green; sky is cyan, so on). These processes can be achieved by some form of automatic, intelligent scene segmentation and material identification. With the use of multiple images at different wavelengths, multispectral information can be used to help identify materials; however, with only a few different spectral bands and complications imposed by variations in conditions, spectral information alone is insufficient. Additional information extracted from the spatial aspect of the image can be used to make a more robust and consistent system.

Of the various spatial properties of an image that can be exploited, we have developed a method utilizing texture to enhance segmentation and object recognition in scene images. In particular, texture is useful for night vision applications since, unlike spectral information, it is basically invariant to environmental conditions. Furthermore, texture can be characterized as a periodic pattern, which enables the use of various mathematical decompositions aiding analysis.

Various methods have been proposed for texture analysis. Haralick *et-al* [6] suggested the use of a gray level co-occurrence matrix that reveals certain properties about the spatial distribution of the gray levels in the texture image. Wallace *et-al* [7] presented that the autocorrelation function of an image can also be used to assess the amount of regularity as well as the fineness/coarseness of texture present in the image. However, these features do not show good performance in segmentation tasks. Markov Random Fields (MRFs) have been popular for modeling and capturing the local (spatial) contextual information. MRF

models have been employed to various image processing applications such as texture synthesis [8], texture classification [9] and texture segmentation [10], [11]. While MRF model captures micro-texture well, it tends to fail with regular and inhomogeneous textures.

Another very useful texture modeling comes from the use of Gabor filtering. The Gabor filters have some desirable optimality properties for texture analysis; for example, their orientation and radial frequency bandwidths are tunable, center frequencies are tunable, allowing achieving optimal joint resolution in space and in spatial frequency. Bovik and Clark [12] proposed a computational approach using 2-D Gabor filters for visible texture analysis. They found the approach is feasible for segmenting both artificial and natural textures in a predictable manner. Thai and Healey [13] proposed measuring color texture by embedding the Gabor filters into an opponent color representation. The method provides a useful structural representation for texture containing significant color variation.

In this paper we present a true color rendering algorithm based on Gabor filter texture analysis over multi-band night vision imagery for material identification. Materials are identified based on their signature that contains both spectral and spatial characteristics. The spectral characteristics include reflective properties (e.g., VNIR, SWIR) and thermal properties (e.g., MWIR, LWIR), and spatial characteristics include the natural texture of background materials in the scene. Ancillary data are also used to enhance the accuracy and reliability of the material identification process.

The algorithm is divided into four sequential main steps. The first step is to apply a set of Gabor filters to the input multi-band imagery to generate a Gabor response signature image cube of spectral and texture characteristics in the scene. The second step is the segmentation of this spectral/texture image cube using unsupervised classification tools. The third step is the identification of the unknown classes in the cube, which is accomplished by comparing to a material database with the aid of the ancillary data. The database contains mainly background materials, which have unique or predictable colors when viewed in the daytime. The algorithm tries to identify the background materials and when successful render those potions of the scene with their unique color. Materials not found in the database are either regarded as unknown targets, and highlighted in the scene, or left as grayscale. In the final step, the color information is combined with brightness image to produce the final color fusion image displayed to the viewer. This brightness image is obtained separately from the input imagery and is created through a standard image fusion method such as a pyramidal [14], wavelet [15], or a simple blending method. In the current paper, a weighted averaging fusion method is used for simplicity. More detailed description of each step is provided in following sections. A conceptual overview of the steps is shown in Figure 1.

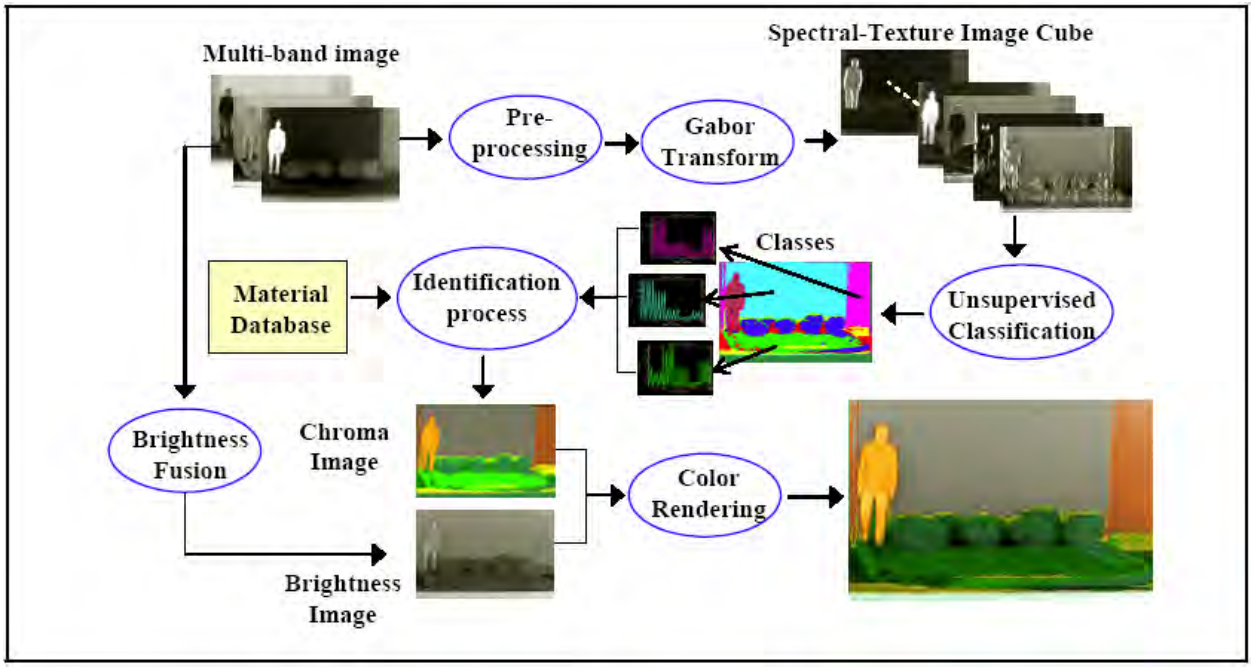

Figure 1. Fusion using color determined by spectral / texture based material identification.

1. Generating Spectral/Texture Gabor Responses

Gabor responses are generated using a set of optimized Gabor filters defined by the Gabor function, which is obtained by modulating a sinusoid with a Gaussian. The following function describes the 2-D Gabor filter;

$$g(x,y,\sigma,\theta,\gamma,\lambda,\psi)=\frac{1}{2\pi\sigma^2}\cdot e^{-\frac{u^2+(\gamma\cdot v)^2}{2\sigma^2}}\cdot\cos(\frac{2\pi u}{\lambda}+\psi) \quad (1)$$

where $u=x\cos\theta+y\sin\theta$ and $v=-x\sin\theta+y\cos\theta$. The aspect ratio λ is typically smaller than one fifth of the filter size to prevent the occurrence of undesired effects at the border among the objects in the image. The appropriate filter size depends on the detail of the feature in the image; for example, the feature size in the image is approximately proportional to the camera focal length. The value θ determines the orientation of the sinusoid, which is related to texture orientation. The scale parameter σ is typically connected to the value of λ as $\sigma=0.56\lambda$. The value γ is typically determined in between 0.5 to 1.0 to control the ellipticity of filter shape. The phase value ψ is set to zero value to give a center-symmetry Gabor function. Methods for designing an efficient set of Gabor filters can be found in [16], [17]

A selection of optimal filters with proper parameter values is crucial to the performance and real-time capability. The selected filters are used in two modes, (i) generating a database of spectral/texture properties for candidate materials, and (ii) applied to spectral imagery to generate a spectral/texture image cube (Gabor responses) from the input imagery. Figure 2 shows an example of how Gabor filters are applied to multi-band imagery to extract different textures in the image. It is noted that we took a color image as a special case of multi-band image for instance. The filter responses in Figure 2 are synonymous to the spectral/texture image cube that is shown in Figure 1.

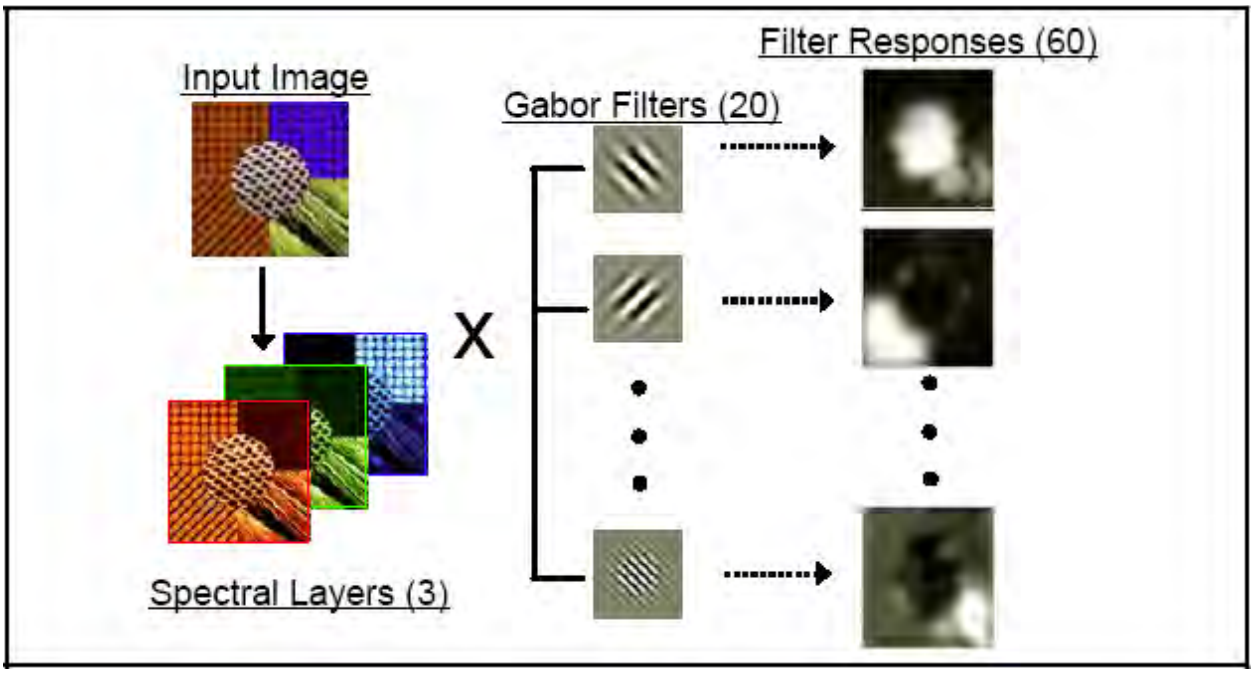

Figure 2. Example of Gabor filter applied to color texture image to extract different textures.

The last step is to combine the spectral and texture images into a well registered image cube for subsequent analysis.

2. Segmentation

In the segmentation process, the spectral/texture image cube is spatially segmented into several clusters (unknown classes) using an unsupervised classification algorithm. As a pre-process, each band of the spectral/texture input cube is smoothed by a Gaussian lowpass filter to suppress the variation of feature vectors within the same spectral/texture region. For the clustering process, the k-means unsupervised algorithm is applied on the feature space to produce a set of initial clusters. As a post-process, a feature similarity of adjacent clusters is computed to allow region merging. We employ our own "Enhanced Canonical Analysis (ECA)" [18] as a similarity measure, which is an enhanced version of Canonical Analysis (CA) based on; (i) optimization of the matrix inversion and (ii) use of multiple iterations. CA is a general technique often used in spectral analysis to find the optimal linear combination of wavelength bands that maximizes the separation (e) of two classes below;

$$e = \frac{\vec{E}^T \Sigma_A \vec{E}}{\vec{E}^T \Sigma_w \vec{E}}. \tag{2}$$

Here, E is the eigenvector, $\boldsymbol{\Sigma}_A$ is the among-classes covariance matrix (that is the covariance matrix between two clusters), and $\boldsymbol{\Sigma}_w$ is the average of the within-class covariance matrices (that is the average of the separate covariance matrices of two classes). Based on the separation index e, the two adjacent clusters are merged if their separation e is under a threshold. Figure 3 shows the graphical overview of entire segmentation process.

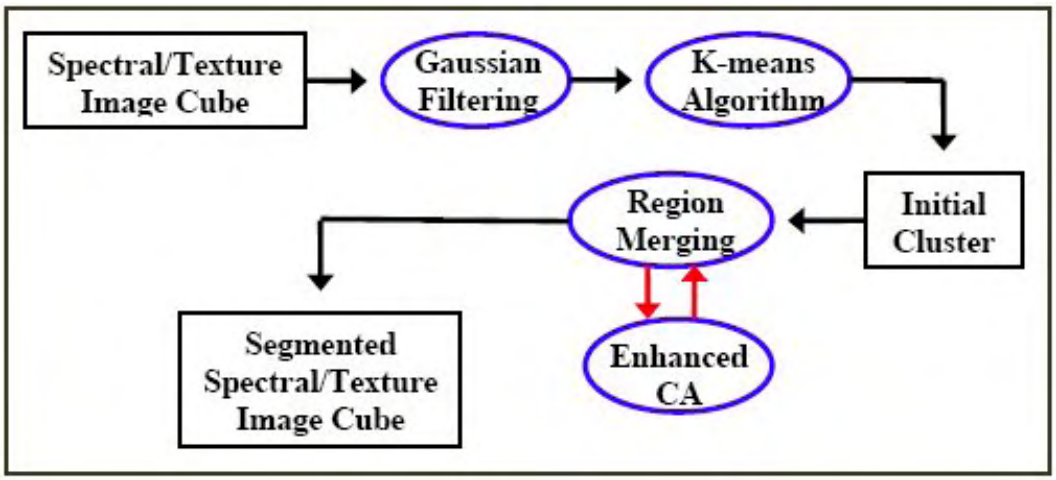

Figure 3. Overview of segmentation process.

3. Material Identification

Once the segmentation process is finished, each unknown class (cluster) is compared to various reference material data in the spectral/texture material database for the purpose of materials identification. ECA, as described in Section 3, is used again to compute the matching probability. In fact, since the separation index *e* in ECA is inversely proportional to the matching probability, a matching model is established using Gaussian Probability Distribution Function (PDF) to convert separation index to probability. Figure 4 shows a Gaussian PDF model for the conversion. The model parameter mean and standard deviation of the Gaussian function are set to 0.0 and 1.089 respectively, which is the result of requiring the probability to be 1 at a separation index of zero, and 0.9 at a separation index of 0.5.

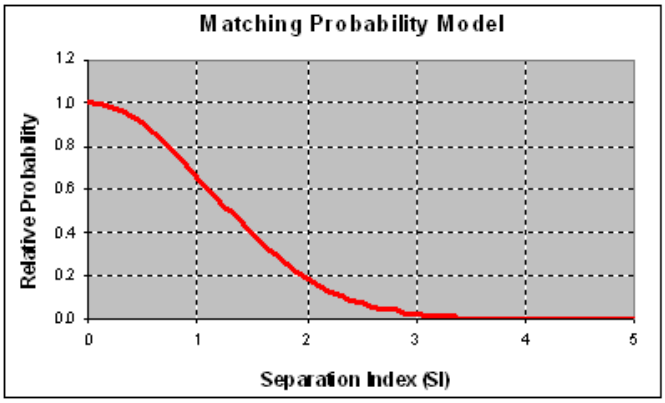

$$P_{Matching} = e^{-\frac{SI^2}{2\sigma^2}}$$

where $\sigma = 1.089221$

Figure 4. Gaussian matching model (Note: SI means the separation index *e*).

The materials in the database consist of mainly natural backgrounds and man-made backgrounds with invariant or predictable colors. For example, vegetation like trees and grass typically have a greenish color, and though they sometimes appear in different shades (even brown) those portions of the scene will be more easily recognized and understood when rendered with a greenish hue. Alternatively, most man-made targets (e.g., vehicles) do not have unique recognizable colors, and are not predictable under various environmental changes. Furthermore since there are many unknown target materials, it is not possible to collect all of those materials into the database a-priori. Therefore the algorithm tries to identify only those background materials existing in the database and render them with their unique colors, while the materials not found in the database are classified as unidentified materials (unknown targets). These

unidentified materials are highlighted in non-natural colors or bounded by their edge during the subsequent color rendering process. Currently we have collected in a sample database several background materials such as tree, grass, soil, dirt, asphalt, concrete, water and sky. The spectral imagery for each material is usually taken at day and night times, which enables the database to be used in two different modes of day or night time operation. The imagery is stored in the database in the form of spectral/texture image cube described in Section 2. The database also stores a color table with unique color value of each material. However those color assignment are somewhat subjective, depending on day or night, seasonal or weather change and different locations. Hence the color table is changeable, and can be replaced by a more suitable table at the time of operation.

The material identification depends on the matching probability between unknown classes and material members in the database. However, we have devised a supplementary means to improve the accuracy of this identification with a knowledge-based inference technique using additional ancillary data. The role of the technique is to determine the likelihood that certain materials exist in the scene. This is particularly important when there are several candidate materials in the database that provide competing matching scores to a given unknown class in the scene segments (i.e., when there are no clear "winners" in terms of matching probability). For example, if GPS indicates the current location is in a forest area, the existence of trees is higher in likelihood than sand, or if an inertial measurement unit (IMU) indicates the viewing angle of the camera is down-looking, the chance of sky existing in the scene would be lower. This concept is further explained below. It is assumed that ancillary data are available such as GPS position of the observer, pointing direction (IMU), and satellite imagery of the local area. To this end the system could rely in the future on various Global Information Grids (GiGs) and specifically Geographic Information System (GIS) Grid Services that include map Services and Sensor Enablement Services [19] using SensorML (Sensor Model language, [20]).

The approach provides quantitative probability of different material presence in a scene based on the ancillary data. Supervised classification is applied to the satellite image to determine which material is present at each pixel. Figure 5 shows IKONOS satellite imagery and its material mapped image of a test scene area where night vision data has been previously collected. In practice, the material mapping on satellite imagery is performed as preprocessing prior to the data collection.

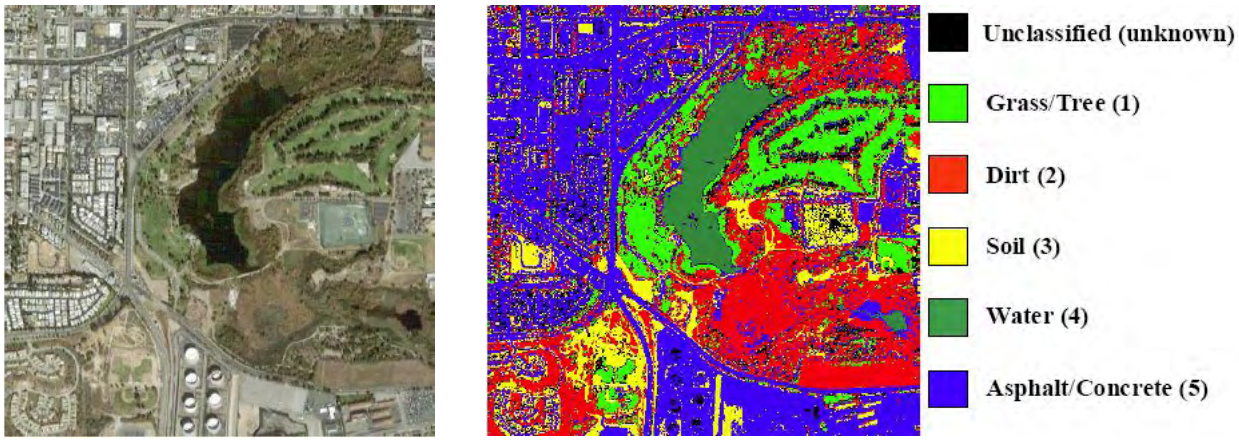

(a) RGB IKONOS Satellite Image **(b) Material Map after Supervised Classification**

Figure 5. Example of technique to determine material abundance as a function of position.

Once the material mapped satellite imagery is prepared, or obtained via the GiG, we can narrow down the image to a detailed geographical region centered near the location where the data is actually being collected. The GPS coordinates are used together with the camera pointing direction and field of view to determine the probability of the scene contents as shown in Figure 6.

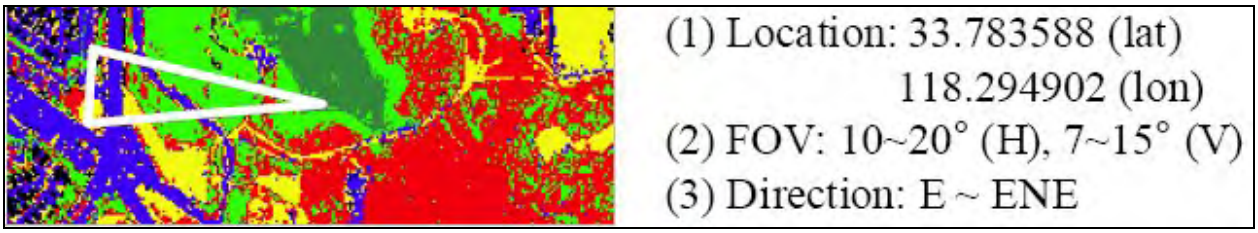

Figure 6. Portion of IKONOS material map with the observer location, viewing direction and field of view.

The probability is determined by counting the number of pixels in the angular field of view with a 1/distance^2 weighting factor. This factor is used so that near objects have high viewing probability and further objects have lower viewing probability. The resulted material probabilities in the scene are shown in Figure 7.

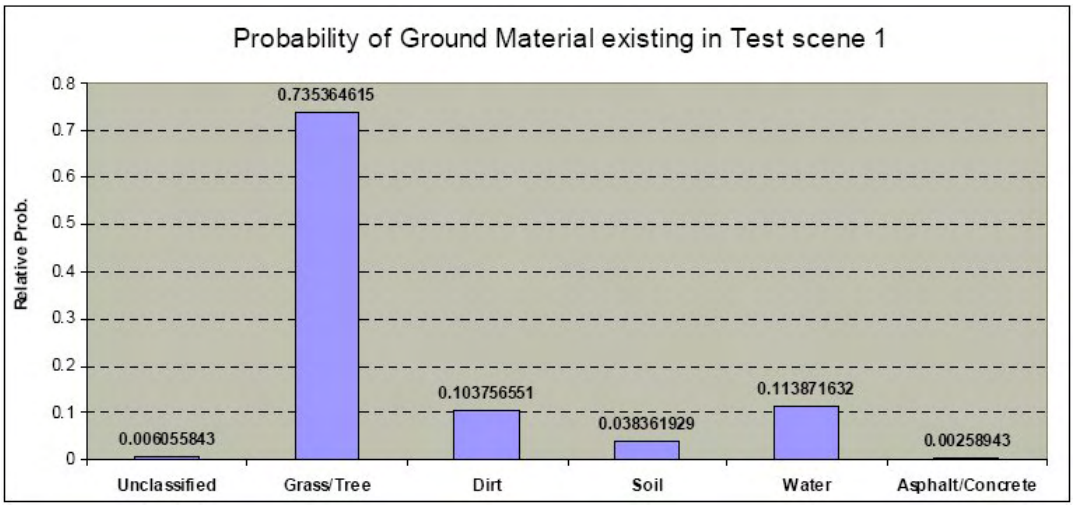

Figure 7. Material probabilities in the scene.

Therefore the matching score between an unknown class in the segmented spectral/textural image cube and a particular material in the database is represented as a score combining database matching probability weighted by scene material presence probability. Mathematically, suppose $\{X_i\}_{i=1}^{p}$ is taken to be a set of unknown classes from a segmentation process in the scene ***S***, and $\{M_j\}_{j=1}^{q}$ is taken to be a set of materials in a given database, then each X_i would be compared to each M_j to score how well they match in terms of probability likelihood, $P(X_i \approx M_j)$, as shown in Figure 4. By combining the likelihood that a given material is in the scene ***S***, $P(M_j \in S)$, with the likelihood that it matches in the database $P(X_i \approx M_j)$, we can derive a combined matching score as:

$$\text{Matching score} = P(X_i \approx M_j) \times P(M_j \in S) \tag{3}$$

Based on the matching scores obtained from Eq. (3), a material M_j with highest matching score to the unknown class X_i is assigned, and its color (chorma) pre-defined for material M_j in the color table is assigned to the class X_i. The class X_i with score below a threshold is classified to unidentified material,

and is assigned to "unidentified" index. An overview of the material identification algorithm is shown in Figure 8 describing use of ancillary data.

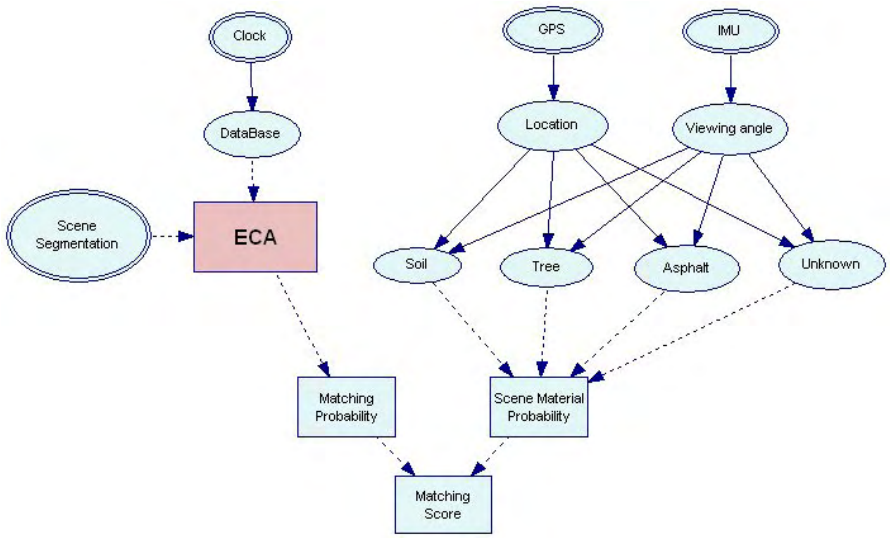

Figure 8. Overall diagram of material identification that utilizes both local spectral/texture data along with ancillary (if available) GIS data.

4. Brightness Fusion and Color Rendering

Once colors are assigned to the identified classes in the segmented scene image, we generate a chroma image using a device independent color space such as HSV or Yuv. The material database has only chroma values (e.g., "HS" or "uv"), which are assigned during material identification. For the unidentified classes, they are assigned to non-natural colors, or not assigned to any color so that they reflect the value of brightness band. Brightness value for a scene is extracted from the actual imagery and not from any table of database. As mentioned above, the brightness image is generated from a combination of the original input images. This process is the typical output of standard fusion techniques that are designed to maximize image content and improve image contrast. Figure 9 shows an example of simple brightness fusion and color rendering on the fused brightness band using true color values in the HSV and Yuv color space. The brightness band (a) is obtained from the combination of the SWIR and LWIR bands of the scene. The color values in (b) and (c) are converted from true RGB values in the scene using HSV and Yuv transformations respectively.

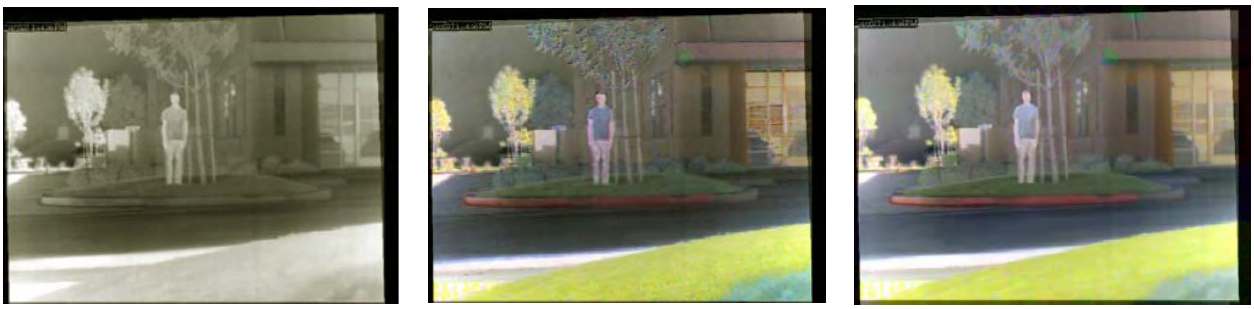

(a) Fused brightness band from SW/LWIR **(b) Color rendered image in HSV** **(c) Color rendered image in Yuv**

Figure 9. Example of brightness fusion and color rendering.

5. Experiments

In this section we present a daytime and a nighttime scenes to test our algorithm. Though the system is designed for nighttime operation, we also conducted the daytime experiment to test daytime color rendering. The imagery was collected by a suite of cameras that span the spectrum from visible to long wave infrared. The specifications of these cameras are listed in Table 1. The daytime scene used for initial testing is shown in Figure 10.

Table 1. Parameters for cameras used to collect sample imagery.

Camera	Make	Wavelength	Lens	Data Format	Comments
Visible	Watec / 232 day-night	0.4 - 0.7 μm	Schneider Cine. 12mm	640 x 480 color jpeg	Can also be used as LLL monochrome V-NIR
SWIR	Sensors U. / SU320MX	1.0 - 1.7 μm	Schneider Xeno. 35mm	320 x 240 8-bit jpeg	Can also be used at night
Dual Band MWIR/LWIR	Raytheon 172	3.0 - 5.0 μm 6.0 - 10.0 μm	Janos Ninox 25mm	256 x 256 12-bit	There are several dead or damaged pixels
LWIR - microbolometer	BAE / MIM500H	7.0 - 14.0 μm	Janos Strix 25mm	320 x 240 14-bit	Integrated into a multi-spectral (MSTIR) system

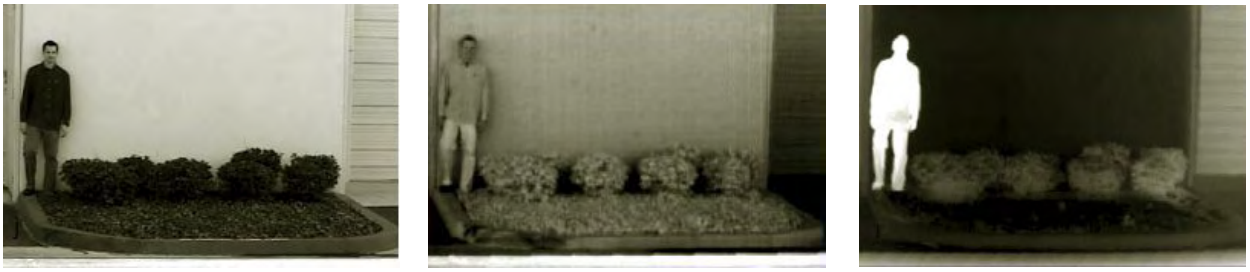

(a) Visible **(b) SWIR** **(c) LWIR**

Figure 10. Multispectral test imagery (3 monochrome bands from each spectral region).

In this experiment, we use 16 Gabor filters built from four different aspect ratios λ and four orientations θ. Table 2 shows the actual values of the parameters used to create the filters. These parameters are optimized for the natural materials in the test data. By applying the set of 16 Gabor filters to each of the 3 input bands, we obtain 48 filter response images that form the complete spectral/texture image cube. Each response image is smoothed by a Gaussian Lowpass filter to suppress the variation of Gabor feature vectors. Then K-means unsupervised classification is applied to the spectral/texture image cube to produce a segmented image. Figure 11(a) shows the result of segmentation using spectral/texture feature (48 band spectral/texture image cube), while (b) shows the segmentation conducted only using spectral information (3 band multispectral imagery).

Table 2. Selection of parameters in Gabor filters.

Parameter	λ	θ (degree)	σ	γ	ψ
Value	3.5, 4.0, 4.5, 5.0	0, 45, 90, 135	2	0.8	0

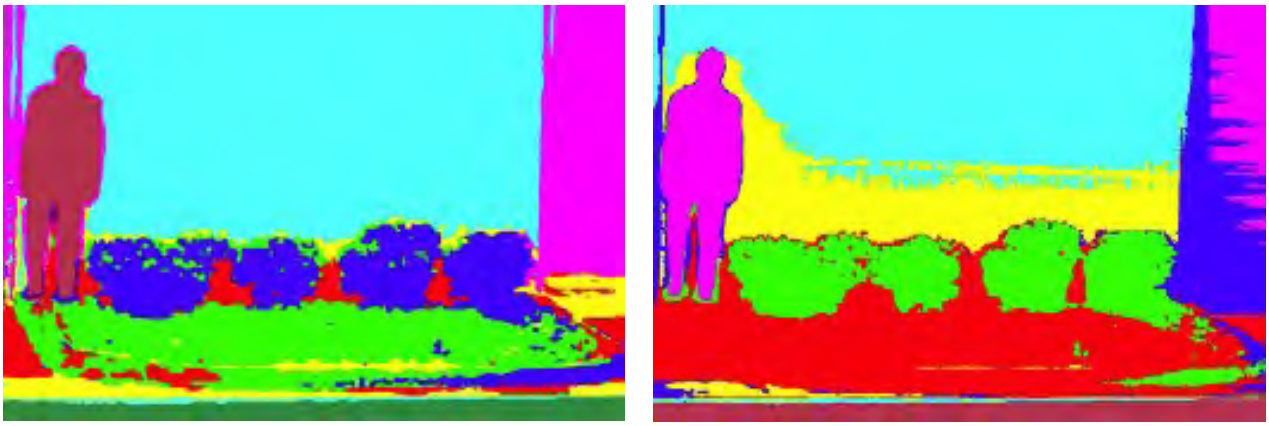

(a) Using Spectral and Texture **(b) Using Spectral only**

Figure 11. Result of segmentations with and without texture feature (no material are identified and no color assignments are applied yet – colors above represent different classes identified by segmentation).

As shown in Figure 11(b), using only spectral information, the roll-up door on the right side of the image and the wall in the background are both mistakenly split into two classes. Adding texture, Figure 11(a), fixes this problem and enables both to be properly classified as being one object each. In addition, with the use of texture, the ivy in the foreground is better segmented from both the surrounding asphalt and the shadows on the wall. Once a class in the test scene is identified to be a material in the database, the chroma value of the material is assigned to the class and every pixel in the class is rendered with that color.

The brightness band is created from one of multispectral bands or combined band obtained from a proper fusion technique. Figure 12 shows the reference color image (a), fused color image using visible band (b), and LWIR band (c) as brightness. The use of visible band helps us to recognize more details of background materials, while LWIR brightness band tends to highlight man-made objects with high temperature in the scene image.

(a) Color Reference **(b) Fused with Visible** **(c) Fused with LWIR**

Figure 12. Color reference image and fused color images with various brightness images.

In both colorization processes, the person is displayed in monochrome because the material database does not include humans as material. In this case the objects that do not exist in the database have only brightness values provided by brightness bands in both cases.

Nighttime scenes fusion tests are shown in Figure 13. The same set of Gabor filters as was used in daytime scene is used for the nighttime scene. Applying the identical segmentation process to these images, we produce image segmentation as shown in Figure 14 (a). In this image, segmented classes

were associated with materials and assigned a color from the library. Figure 14(b) is the brightness band obtained from average of three spectral bands, Visible, SWIR and LWIR in Figure 13.

(a) Visible **(b) SWIR** **(c) LWIR**

Figure 13. Multispectral test scenes.

(a) Segmentation using spectral and texture **(b) Brightness image fused from spectral images**

Figure 14. Results of segmentation and brightness fusion.

Finally, the color bands are fused with the brightness band to produce final color fused image. Figure 15(a) shows the fused color image, where the color values are taken from Figure 14(a) and the lightness values from Figure 14(b). A color image of the same scene, Figure 15(b), captured at nighttime with a color EMCCD camera system, is shown for reference.

(a) Color fused image **(b) Reference color image**

Figure 15. Comparison of true color rendered image to actual nighttime color image.

6. Summary

We have developed a general technique for true color rendering using multiband night vision imagery that can be used to improve scene understanding and situational awareness. The algorithm is based on material identification using a knowledge based inference that considers material database matching together with expected scene content. We implemented the technique of Gabor filtering to add the texture property, which improves the performance of material database matching. We also developed a technique that utilizes ancillary data such as GPS, IMU, satellite imagery and other GIS for material probability determination in the scene, which helps the material database matching and eventually increases the accuracy of the material identification. This approach will take advantage of Global Information Grids that include Geographical Information System Grid Services, and other sensor Model Language components. Two experiments were performed with daytime and nighttime real image data captured with multiband camera system, and show that background materials are correctly assigned with recognizable colors in the scene. The capability to present night time scene in true recognizable colors can drastically improve human performance under difficult night operations, by reducing reaction time, and enhancing scene understanding.

For the future work, the probability of scene contents accuracy will be improved by incorporating the 3D information of the scene. The 3D view of the scene aides more accurate determination of scene content by considering the problems such as “how far does the field of view extend?” or “is the scene dominated by tall objects in the fore ground?” Such technique will take advantage of the rapid expansion of global information grids across the DoD, Network Centric Operations and Warfare.

Acknowledgement

This research was supported by the Army Research Office under grant W911NF-08-C-0127.

References

[1] J. A.A. Cavanillas, "The role of Color and False Color in Object Recognition with Degraded and Non-Degraded Images," Thesis, Naval Postgraduate School Monterey, CA (Sep. 1999).

[2] M.T. Sampson, "An Assessment of the Impact of Fused Monochrome and Fused Color Night Vision Displays on Reaction Time and Accuracy in Target Detection," Thesis, Naval Postgraduate School Monterey, CA (Sep. 1996).

[3] M.A. Hogervorst, and A. Toet, "Method for applying daytime colors to nighttime imagery in realtime," Proc. of SPIE Vol. 6974, 697403-1, 2008.

[4] A. Toet and J. Walraven, "New false color mapping for image fusion," Optical Engineering, 1996.

[5] D.A. Fay, A.M. Waxman, M. Aguilar, D.B. Ireland, J.P. Racamato, W.D. Ross, W.W. Streilein, and M.I. Braun, "Fusion of Multi-Sensor Imagery for Night Vision: Color Visualization, Target Learning and Search," Proc. Of FUSION 2000, Vol.1, pp. 303-310, 2000.

[6] R.M. Haralick, K. Shanmugan, and I. Dinstein, "Textural Features for Image Classification," IEEE Transaction on System, Man, and Cybernetics, Vol. 3, No.6, pp. 610-621, 1973.

[7] C. S.A. Wallace, J.M. Watts, and S.R. Yool, "Characterizing the spatial structure of vegetation communities in the Mojave Desert using geostatistical techniques," Computer & Geostatistics 26: 397-410, 2000.

[8] G.C. Cross, and A.K. Jain, "Markov Random Field Texture Models," *IEEE Transactions on Pattern Analysis and Machine Intelligence*, PAMI-5, pp. 25-39, 1983.

[9] R. Chellappa, and S. Chatterjee, "Classification of Textures Using Gaussian Markov Random Fields," *IEEE Transactions on Acoustic, Speech and Signal Processing*, ASSP-33, pp. 959-963, 1985.

[10] C.W. Therrien, "An Estimation-Theoretic Approach to Terrain Image Segmentation," Computer Vision, Graphics, and Image Processing, 22, pp. 313-326, 1983.

[11] Z. Kato, and T. Pong, "A Markov random field image segmentation model for color textured images," Image and Vision Computing 24, pp. 1103-1114, 2006.

[12] A.C. Bovik and M. Clark, "Multichannel Texture Analysis Using Localized Spatial Filters," IEEE Transactions on Pattern Analysis and Machine Intelligence, Vol. 12 No.1 (Jan. 1990).

[13] B. Thai, and G. Healey, "Modeling and classifying symmetries using a multiscale opponent color representation," IEEE Trans. On PAMI, 20(11): 1224-1235, 1998.

[14] E. Adelson, C. Anderson, J. Bergen, P. Burt, and J. Ogden, "Pyramid methods in image processing," RCA Engineer 29, 33-41, 1984.

[15] S.G. Mallat, "A theory for multiresolution signal decomposition: The wavelet representation," IEEE Trans. Pattern Anal. Machine Intell., vol. PAMI-11, pp. 674-693, 1989.

[16] T. Weldon, W. Higgins, and D. Dunn, "Efficient Gabor filter design for texture segmentation," Pattern Recognition 29 (12), 2005-2016, 1996.

[17] B. Manjunath, and W. Ta, "Texture features for browsing and retrieval of image data," IEEE Trans. Pattern Anal. Machine Intell., 18 (8), 837-842, 1996.

[18] K. Lee, J. Kriesel, N. Gat, and P. Willson, "Optimal Multispectral Thermal IR Band Selection for Target Contrast Enhancement and Color Scene Rendering," Military Sensing Symposia (MSS) Specialty Group on Passive Sensors. Nellis AFB, NV. Feb. 2008.

[19] G. Fox, A. Ho, S. Pallickara, M. Pierce, W. Wu "Grids for the GiG and Real Time Simulations," http://grids.ucs.indiana.edu/ptliupages/publications/gig/DSRTOct05.pdf.

[20] http://www.opengeospatial.org/standards/sensorml, and http://vast.uah.edu/index.php?option=com_content&view=article&id=14&Itemid=52.